ISVR, Southampton, UK
ACTIVE 2002
2002 July 15-17

OPTIMIZATION STRATEGY FOR ACTUATOR AND SENSOR PLACEMENT IN ACTIVE STRUCTURAL ACOUSTIC CONTROL

M.H.H. Oude Nijhuis and A. de Boer

University of Twente, Faculty of Mechanical Engineering
P.O. Box 217, 7500 AE Enschede, The Netherlands,
Email: m.h.h.oudenijhuis@wb.utwente.nl

Introduction

Over the past decades, active control methods have become valuable tools besides passive methods for attenuating the sound radiation of structures. The goal of a control system is to cancel the response generated by a disturbance or primary source by introducing one or several secondary controlled source(s). In *active structural acoustic control* (ASAC), actuators are directly attached to the structure, and a reduction of the radiated sound is achieved by changing the vibrational behaviour of the structure [1]. Furthermore, often a control system is used with sensors that measure vibrations instead of acoustic pressure. Piezoelectric materials are often used in ASAC as actuator or sensor, mainly because they can be bonded directly to the structure, not requiring a back support.

For linear systems the sound radiated by a structure is equal to the sum of the sound field if only the disturbance were active (primary field) and the sound field if only the control input(s) were active (secondary field). So in principle a structure will radiate no sound if the secondary sound field matches the primary field in time and space[1]. The quality of the temporal match is determined by the control algorithm and hardware, whereas the spatial match is also determined by the location and characteristics of the actuators and sensors. Optimization of sensor and actuator locations for ASAC is the topic of this work.

Obviously optimization for ASAC requires a structural-acoustic model representing the dynamical behaviour of the system. The early works on optimization for ASAC, such as those of Clark and Fuller [2] and of Wang, Burdisso and Fuller [3], consider simply supported rectangular plates which can be represented by analytical models. Unfortunately, many practical problems cannot be described with analytical models. Since active control is more valuable in the low frequency region, the *Finite Element Method* (FEM) can be applied for such problems. Furthermore, it is then possible the include the actuator and sensor dynamics. Optimization studies using FEM models can be found for instance in the works of Varadan, Kim and Varadan [4, 5] and De Fonseca, Sas and Van Brussel [6]. The first paper considers plate structures with piezoelectric patches, and FEM models including the actuator dynamics. However, optimal locations with respect to minimal sound radiation are determined only at discrete frequencies. In reference [6] a broad-band frequency range is considered, but only point force actuators are

[1] Either the temporal match or the spatial match should be shifted 180 degrees (anti-phase)

applied.

In this work an optimization strategy is presented where the structure is modelled with the finite element method, and a broad-band frequency range is considered. The FEM model describes the structural dynamics of the system including the dynamics of piezoelectric patches. The structural model is combined with an acoustical model based on the Rayleigh integral. In order to reduce computational effort, model reduction techniques are applied. The optimization routine uses a closed-loop model of the system, where a simplified control algorithm is applied to model the controller. The *genetic algorithm* (GA) is used as the optimization tool. The strategy is applied to determine the optimal actuator and sensor location corresponding with minimal free field sound radiation of a clamped rectangular plate. The actuator is a piezoelectric patch, whereas several sensor types are used. The results are compared with a simple placement strategy which uses the mode shapes of the plate.

Modelling

The model used in the optimization strategy is presented in three parts. The structural dynamics are described with a FEM model, where the piezoelectric patch(es) are included in the model. FEM models have in general a large number of degrees of freedom (DOF). A model reduction technique is described to reduce the number of DOF and thus reduce the computational effort. Next a model is given for the sound radiation based on the Rayleigh integral. Note that this model is only valid for plate-like structures, whereas the structural model can be used to model any coupled structural-piezoelectric dynamical system. It is however possible to replace the acoustical model by a more advanced model for more complex structures, e.g. a boundary element model. The optimization routine uses a closed-loop model of the system, where optimal control theory is applied to model the controller.

Structural Model. The linear FEM equations of motion for a coupled structural-piezoelectric system are given by

$$\begin{bmatrix} \mathbf{M}_{uu} & \mathbf{0} \\ \mathbf{0} & \mathbf{0} \end{bmatrix} \begin{Bmatrix} \ddot{\mathbf{u}} \\ \ddot{\boldsymbol{\phi}} \end{Bmatrix} + \begin{bmatrix} \mathbf{C}_{uu} & \mathbf{0} \\ \mathbf{0} & \mathbf{0} \end{bmatrix} \begin{Bmatrix} \dot{\mathbf{u}} \\ \dot{\boldsymbol{\phi}} \end{Bmatrix} + \begin{bmatrix} \mathbf{K}_{uu} & \mathbf{K}_{u\phi} \\ \mathbf{K}_{\phi u} & \mathbf{K}_{\phi\phi} \end{bmatrix} \begin{Bmatrix} \mathbf{u} \\ \boldsymbol{\phi} \end{Bmatrix} = \begin{Bmatrix} \mathbf{f} \\ \mathbf{g} \end{Bmatrix}, \qquad (1)$$

where $\mathbf{u}$ is the vector with nodal structural displacements and rotations, and $\boldsymbol{\phi}$ is the vector with nodal voltages. Matrices $\mathbf{M}_{uu}$, $\mathbf{C}_{uu}$, and $\mathbf{K}_{uu}$ are respectively the structural mass, damping and stiffness matrix. Matrix $\mathbf{K}_{\phi\phi}$ is the dielectric stiffness matrix. The piezoelectric coupling arises in the piezoelectric stiffness matrices $\mathbf{K}_{u\phi}$ and $\mathbf{K}_{\phi u} = \mathbf{K}_{u\phi}^{\mathrm{T}}$. The external loads are stored in $\mathbf{f}$, i.e. the vector with nodal structural forces, and $\mathbf{g}$, which is the vector with nodal electrical charges. The main assumption made in the derivation of Eqs. (1) is that the electrical field behaves quasi-statically. Note that $\mathbf{u}$ contains the nodal displacements of the structure as well as the nodal displacements of the piezoelectric material.

In general FEM models contain a large number of degrees of freedom (DOF). A model reduction technique is applied to restrict simulation times. Here only a short summary of the method is given, more details can be found in reference [7]. In a control setup piezoelectric materials can be used either as actuator or sensor. In case the patch is used as actuator the electrode potential is prescribed, whereas for a sensor the potential is free. It is convenient to divide the vector with nodal voltages into two parts: $\boldsymbol{\phi} = \{\boldsymbol{\phi}^p \ \boldsymbol{\phi}^f\}^{\mathrm{T}}$, where $\boldsymbol{\phi}^p$ is the vector with *prescribed* nodal voltages, and $\boldsymbol{\phi}^f$ contains the *free* nodal voltages. Substitution of this

vector into Eqs. (1) gives

$$\begin{bmatrix} \mathbf{M}_{uu} & \mathbf{0} & \mathbf{0} \\ \mathbf{0} & \mathbf{0} & \mathbf{0} \\ \mathbf{0} & \mathbf{0} & \mathbf{0} \end{bmatrix} \begin{Bmatrix} \ddot{\mathbf{u}} \\ \ddot{\boldsymbol{\phi}}^p \\ \ddot{\boldsymbol{\phi}}^f \end{Bmatrix} + \ldots + \begin{bmatrix} \mathbf{K}_{uu} & \mathbf{K}^p_{u\phi} & \mathbf{K}^f_{u\phi} \\ \mathbf{K}^p_{\phi u} & \mathbf{K}^{pp}_{\phi\phi} & \mathbf{K}^{pf}_{\phi\phi} \\ \mathbf{K}^f_{\phi u} & \mathbf{K}^{fp}_{\phi\phi} & \mathbf{K}^{ff}_{\phi\phi} \end{bmatrix} \begin{Bmatrix} \mathbf{u} \\ \boldsymbol{\phi}^p \\ \boldsymbol{\phi}^f \end{Bmatrix} = \begin{Bmatrix} \mathbf{f} \\ \mathbf{g}^p \\ \mathbf{g}^f \end{Bmatrix} . \quad (2)$$

For ease of writing the damping forces are omitted in this equation. The reduction method which is applied is a *mode superposition method*. First the free electrical DOF are eliminated with static condensation. The results is an equation of motion in terms of the structural displacements, i.e.

$$\mathbf{M}_{uu}\,\ddot{\mathbf{u}} + \mathbf{C}_{uu}\,\dot{\mathbf{u}} + \mathbf{K}^{\star}_{uu}\,\mathbf{u} = \mathbf{f}^{\star} . \quad (3)$$

In this equation the effective stiffness matrix $\mathbf{K}^{\star}_{uu}$ and force vector $\mathbf{f}^{\star}$ are defined as,

$$\mathbf{K}^{\star}_{uu} = \mathbf{K}_{uu} - \mathbf{K}^f_{u\phi}\big(\mathbf{K}^{ff}_{\phi\phi}\big)^{-1}\mathbf{K}^f_{\phi u} , \quad (4)$$

$$\mathbf{f}^{\star} = \mathbf{f} - \mathbf{K}^f_{u\phi}\big(\mathbf{K}^{ff}_{\phi\phi}\big)^{-1}\mathbf{g}^f - \mathbf{K}^{p\star}_{u\phi}\,\boldsymbol{\phi}^p , \quad (5)$$

where $\mathbf{K}^{p\star}_{u\phi} = \mathbf{K}^p_{u\phi} - \mathbf{K}^f_{u\phi}\big(\mathbf{K}^{ff}_{\phi\phi}\big)^{-1}\mathbf{K}^{fp}_{\phi\phi}$. Equation 5 shows that all applied electrical loads, i.e. nodal charges and prescribed nodal voltages, are transformed to structural loads. Once the structural displacements have been solved, the free electrical DOF can be calculated with

$$\boldsymbol{\phi}^f = \big(\mathbf{K}^{ff}_{\phi\phi}\big)^{-1}\Big[\mathbf{g}^f - \mathbf{K}^f_{\phi u}\,\mathbf{u} - \mathbf{K}^{fp}_{\phi\phi}\,\boldsymbol{\phi}^p\Big] . \quad (6)$$

In the mode superposition method, the response is expanded in terms of the undamped eigenvectors or mode shapes (modes) of the problem. The solution of the undamped eigenvalue problem comprises n_d angular eigenfrequencies ω_i and corresponding eigenvectors $\hat{\mathbf{u}}_i$ ($i = 1 \ldots n_d$), where n_d is the total number structural DOF in the model. Following the method of modal superposition, the solution of Eq. (3) is written as

$$\mathbf{u} = \sum_{i=1}^{n_d} \hat{\mathbf{u}}_i q_i = \boldsymbol{\Psi}_u\,\mathbf{q} , \quad (7)$$

where $\boldsymbol{\Psi}_u$ is a matrix with the structural mode shapes, stored column wise, and $\mathbf{q}$ is the column vector with modal participation factors. Substitution of this solution into Eq. (3) and multiplying through by $\boldsymbol{\Psi}^{\mathrm{T}}_u$ leads to the uncoupled generalized equations of motion:

$$\ddot{q}_i + 2\xi_i\omega_i\,\dot{q}_i + \omega_i^2\,q_i = \hat{\mathbf{u}}_i^{\mathrm{T}}\mathbf{f}^{\star} , \qquad i = 1 \ldots n_d . \quad (8)$$

It is here assumed that the damping is *classical*, which means that the mode shapes are decouple the damping matrix. Note that ξ_i is the modal damping ratio for mode i.

A good estimate of the response in a limited frequency band $\omega \in [\omega_0, \omega_1]$ is obtained when only a small number of mode shapes $m \ll n_d$ is taken into account in summation (7). A consequence of truncating the modal expansion is that it can lead to errors in prediction the response near the anti-resonance frequencies, or in control theory referred to as *zeros* [8]. This is because the mode shapes with eigenfrequencies outside the frequency range of interest also contribute to the frequency response in the range $[\omega_0, \omega_1]$. This contribution is especially significant in the off-resonance regions. The concept of *residual flexibility* improves the accuracy of the truncated

expansion. The exact solution of Eq. (3) when all variables show harmonic time dependency can be written as

$$\hat{\mathbf{u}} = \sum_{i=1}^{m} \hat{\mathbf{u}}_i \hat{q}_i + \sum_{i=m+1}^{n_d} \hat{\mathbf{u}}_i \hat{q}_i \,, \qquad \text{where} \qquad \hat{q}_i = \frac{\hat{\mathbf{u}}_i^{\mathrm{T}} \mathbf{f}^\star}{-\omega^2 + 2\mathrm{j}\xi_i\omega_i\,\omega + \omega_i^2} \,. \tag{9}$$

In the case of standard modal reduction, the second right-hand-side term is neglected. Since the maximum frequency in the range of interest $[\omega_0, \omega_1]$ is much smaller than the natural eigenfrequencies for modes satisfying $i > m$, the system response is well approximated by

$$\hat{\mathbf{u}} \approx \sum_{i=1}^{m} \frac{\hat{\mathbf{u}}_i \hat{\mathbf{u}}_i^{\mathrm{T}} \mathbf{f}^\star}{-\omega^2 + 2\mathrm{j}\xi_i\omega_i\,\omega + \omega_i^2} + \sum_{i=m+1}^{n_d} \frac{\hat{\mathbf{u}}_i \hat{\mathbf{u}}_i^{\mathrm{T}} \mathbf{f}^\star}{\omega_i^2} \,. \tag{10}$$

In this approximation the high frequency modes ($i > m$) contribute statically to the system response, whereas the low frequency modes ($i \leq m$) respond dynamically. The second right-hand-side term is called the residual mode. This term can be expressed in terms of the static response and low frequency mode contributions. The modal expansion of the static response simply follows after inserting $\omega = 0$ into Eq. (9). Now the approximate solution becomes

$$\hat{\mathbf{u}} \approx \sum_{i=1}^{m} \frac{\hat{\mathbf{u}}_i \hat{\mathbf{u}}_i^{\mathrm{T}} \mathbf{f}^\star}{-\omega^2 + 2\mathrm{j}\xi_i\omega_i\,\omega + \omega_i^2} + \mathbf{u}_0 - \sum_{i=1}^{m} \frac{\hat{\mathbf{u}}_i \hat{\mathbf{u}}_i^{\mathrm{T}} \mathbf{f}^\star}{\omega_i^2} \,. \tag{11}$$

Solution $\hat{\mathbf{u}}$ is now written in terms of modes $i = 1 \ldots m$ and the static response $\mathbf{u}_0$. So the cost for a more accurate approximation is that a static response analysis has to be performed.

Acoustical Model. The radiated sound power is often used in ASAC as performance metric for the controller. A model for calculation of this quantity for plate structures is given here. The time-averaged radiated acoustic power through an area S can be expressed as

$$\bar{W} = \frac{1}{2} \operatorname{Re} \left(\int_S p(\mathbf{r}_s)\, v_n^*(\mathbf{r}_s)\, \mathrm{d}S \right) \,, \tag{12}$$

where $p(\mathbf{r}_s)$ and $v_n(\mathbf{r}_s)$ denote respectively the surface pressure and the normal velocity on the structure at position vector $\mathbf{r}_s$. The normal velocity distribution is known from the analysis described in the previous section. It is hereby assumed that the vibration of the structure is not affected by the surrounding medium. In the current work the analysis is restricted to a plate in an infinite baffle, i.e. the Rayleigh integral can be used to model the acoustic field. The Rayleigh integral [9] is given by

$$p(\mathbf{r}) = \frac{\mathrm{j}\omega\rho_0}{2\pi} \int_S v_n(\mathbf{r}_s) \frac{\mathrm{e}^{-\mathrm{j}k|\mathbf{r}-\mathbf{r}_s|}}{|\mathbf{r}-\mathbf{r}_s|}\, \mathrm{d}S \,, \tag{13}$$

where ρ_0 is the mean density of the acoustic medium, $k = \omega/c_0$ is the acoustic wave number with c_0 the undisturbed speed of sound. Because there is normally no closed form solution available, the Rayleigh integral and thus the expression for the radiated sound power are discretised. The surface is divided into l elementary radiators (pistons) of equal size. It is assumed that the velocity and pressure fields across each radiator are constant. Then Eq. (12) reduces to

$$\bar{W} = \frac{S_e}{2} \operatorname{Re} \left(\mathbf{v}_n^{\mathrm{H}}\, \mathbf{p} \right) \,, \tag{14}$$

where $\mathbf{p}$ and $\mathbf{v}_n$ are the vectors with the surface pressure and normal velocity of the elementary radiators, S_e is the surface of an elementary radiator. Discretisation of the Rayleigh integral leads to a linear relation of the form

$$\mathbf{p} = \mathbf{Z}\,\mathbf{v}_n\,, \qquad \text{with} \qquad Z_{ij} = \frac{\mathrm{j}\omega\rho_0 S_e}{2\pi}\,\frac{\mathrm{e}^{-\mathrm{j}k|\mathbf{r}_i-\mathbf{r}_j|}}{|\mathbf{r}_i-\mathbf{r}_j|}\,, \qquad i,j = 1\ldots l\,. \tag{15}$$

The pressure is here evaluated on the surface, meaning that the diagonal elements of impedance matrix $\mathbf{Z}$ are singular ($i = j$). The expression for the time-averaged radiated sound power now becomes

$$\bar{W} = \frac{S_e}{2}\,\mathrm{Re}\left(\mathbf{v}_n^{\mathrm{H}}\,\mathbf{Z}\,\mathbf{v}_n\right) = \mathbf{v}_n^{\mathrm{H}}\,\mathbf{R}\,\mathbf{v}_n\,, \tag{16}$$

where $\mathbf{R} = (S_e/2)\mathrm{Re}(\mathbf{Z})$ is the so-called radiation resistance matrix. Because only the real part of the impedance matrix is used for evaluation of the radiation matrix, no singularity is present.

Below coincidence, i.e. $kL < 1$ with L the characteristic length scale of the plate, the structural modes do not contribute independently to the radiated sound power. Above coincidence, the structural modes radiate more or less independently. In the low frequency range ($kL < 1$), a set of vibration patterns can be defined which do radiate independently, the so called radiation mode shapes [10, 11, 12]. The radiation modes follow from a singular value decomposition of the radiation resistance matrix:

$$\mathbf{R} = \mathbf{\Sigma}^{\mathrm{T}}\,\mathbf{\Lambda}\,\mathbf{\Sigma}\,, \tag{17}$$

where $\mathbf{\Sigma}$ is the matrix with radiation modes, stored row-wise, and $\mathbf{\Lambda}$ is the diagonal matrix with radiation efficiencies. Both matrices are real and depend on frequency. The radiation efficiencies fall off very rapidly with increasing mode order in the low frequency range. Hence it is possible to approximate the sound power with only a small number of radiation modes n_r:

$$\bar{W} \approx \mathbf{v}_n^{\mathrm{H}}\tilde{\mathbf{\Sigma}}^{\mathrm{T}}\,\tilde{\mathbf{\Lambda}}\,\tilde{\mathbf{\Sigma}}\,\mathbf{v}_n\,, \tag{18}$$

where $\tilde{\mathbf{\Sigma}}$ and $\tilde{\mathbf{\Lambda}}$ now include only n_r modes and efficiencies.

Control Algorithm. Optimal control theory determines the optimal response with respect to a quadratic error criterion when controlling a linear system (see for instance Nelson and Elliott[13]). It gives the optimal control performance, irrespective of the control algorithm, in case of a quadratic cost function. The frequency domain response of a linear system subjected to a number of a disturbance and control inputs can be written as

$$\mathbf{y} = \mathbf{H}_d\,\mathbf{f}_d + \mathbf{H}_c\,\mathbf{f}_c\,, \tag{19}$$

where $\mathbf{y}$ is the vector with outputs which are minimized, e.g. plate displacements or pressures. Vectors $\mathbf{f}_d$ and $\mathbf{f}_c$ are the disturbance and control input vectors, respectively, and, $\mathbf{H}_d$ and $\mathbf{H}_c$ are transfer matrices which relate the disturbance and control inputs to the response. The error criterion is defined as

$$J = \mathbf{y}^{\mathrm{H}}\,\mathbf{W}\,\mathbf{y} + \beta\,\mathbf{f}_c^{\mathrm{H}}\mathbf{f}_c\,, \tag{20}$$

where $\mathbf{V}$ is the performance weighting matrix and β is a control effort penalty. The control input vector which minimizes objective equation (20) is given by

$$\mathbf{f}_c^{\mathrm{opt}} = -\left(\mathbf{H}_c^{\mathrm{H}}\mathbf{W}\,\mathbf{H}_c + \beta\,\mathbf{I}\right)\,\mathbf{H}_c^{\mathrm{H}}\mathbf{W}\,\mathbf{H}_d\,\mathbf{f}_d\,. \tag{21}$$

Optimization Strategy

The foregoing model can be used find optimal values of several model parameters (design variables). Obviously an object function must be defined which determines the quality of a certain set of design values. In genetic optimization the object function is often called the *fitness function*. Here the focus in on finding the actuator and sensor locations corresponding with minimal sound radiation in the closed-loop case. Furthermore sound reduction should be achieved in a broad-frequency range. The fitness function is defined as

$$F = \int_{\omega_0}^{\omega_1} \bar{W}(\omega)\,\mathrm{d}\omega \approx \sum_{i=1}^{n_\omega - 1} \frac{\omega_{i+1} - \omega_i}{2} \left[\bar{W}(\omega_i) + \bar{W}(\omega_{i+1})\right] . \tag{22}$$

The radiated sound power $\bar{W}$ is only available at discrete frequencies. Therefore, this integral can only be evaluated numerically, here according to the trapezoidal rule. There exist numerous methods to minimize Eq. (22). In this work genetic optimization is applied, mainly because the method is capable of minimizing multi-modal object functions, i.e function with several minima.

Genetic Algorithm. Genetic algorithms search within the design space for the best solution, hereby simulating a survival of the fittest strategy. Here the genetic algorithm (GA) used in this work is briefly discussed, more thorough discussions on genetic optimization can be found in references [14, 15].

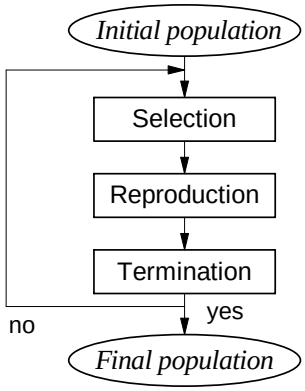

GA features	
Chromosomes	*Floating point*
Initial population	*Random*
Selection	*Normalized geometric*
Crossover	*Arithmetic*
Mutation	*Non-uniform*
Termination	*Maximum generation*

Figure 1: *Schematic representation of the genetic algorithm.*

The genetic algorithm is summarized in Fig. 1. A *floating point representation* of each chromosome or individual within the design space is used. The early genetic algorithms used binary representations but in reference [15] it is shown that floating point based algorithms are more efficient in terms of CPU time. The genetic algorithm must be provided an *initial population*, where a population refers to a set of individuals. The initial population is randomly generated.

The initial population is passed to a *selection* procedure. All individuals have a change of being selected and one individual can be selected more than once. In many selection methods a probability of selection, P_i, is assigned to each individual i, based on its fitness. The cumulative probability is defined as $C_i = \sum_{j=1}^{i} P_j$. An individual i is selected if $C_{i-1} < U(0,1) \leq C_i$, where $U(0,1)$ is random number between 0 and 1. In this way n_p individuals are passed to

a new population, with n_p the population size. Various methods exist to assign probabilities. Here *normalized geometric ranking* is applied, where P_i is based on the rank of the solutions:

$$P_i = \frac{q(1-q)^{r-1}}{1-(1-q)^{n_p}}\,, \tag{23}$$

where q is the probability of selecting the best individual, and, r is the rank of individual i (where one is the best).

Reproduction with genetic operators is the basic search mechanism. With the *crossover* and *mutation* operators new individuals are created based on an existing solution. Crossover takes two individuals (randomly selected) and produces two new individuals whereas mutation alters one individual. Here the *arithmetic* crossover scheme is applied, which produces two complementary linear combinations of two individuals i and j according to

$$\mathbf{x}_i' = r\,\mathbf{x}_i + (1-r)\,\mathbf{x}_j\,, \tag{24}$$

$$\mathbf{x}_j' = (1-r)\,\mathbf{x}_i + r\,\mathbf{x}_j\,, \tag{25}$$

where $\mathbf{x}_i$ is an original chromosome, $\mathbf{x}_i'$ is the new chromosome, and r is a random number between zero and one. Mutation alters one gene (design variable) in the chromosome representing one individual. The *non-uniform* mutation scheme used in this work selects randomly an individual, and sets one design variable bounded by $[a_k, b_k]$ to a non-uniform random number:

$$x_k' = \begin{cases} x_k + (b_k - x_k) f(n_g) & \text{if} \quad i = j, r_1 < 0.5 \\ x_k - (x_k + a_k) f(n_g) & \text{if} \quad i = j, r_1 \geq 0.5 \\ x_k & \text{if} \quad i \neq j \end{cases} \tag{26}$$

where $f(N_g) = (r_2(1 - g/n_g))^b$, n_g is the total number of generations, g is the current generation, b is a shape parameter, and r_1 a r_2 are random numbers. Initially this mutation operator searches the design space uniformly ($g \ll n_g$), but more locally as the number of generations increases.

The genetic algorithm passes several generations while selecting and reproducing individuals. In general the entire population will converge to a single solution. The algorithm is forced to stop when a certain *termination* criterion is met, here if a specified number maximum number of generations has passed.

Implementation

The analysis packages ANSYS and MATLAB are used for implementation of the strategy presented in the previous sections. Calculation of the fitness of a single individual requires the following steps. First a modal analysis and static analyses of a plate structure with piezoelectric patches are performed in ANSYS. To account for the residual flexibility a static analysis must be done for each disturbance and control input. The FEM analysis results are imported in MATLAB, where the reduced model and sound radiation model are defined. It is noted that the structural mesh and acoustical mesh (number of radiators) are not equal. The radiation matrix is calculated only once, and the FEM results are mapped on the acoustical mesh every time the fitness function is evaluated. The optimal control input and response for a certain objective function is determined. Besides the eigenfrequencies and modeshapes also piezoelectric stiffness matrices are required to define the reduced model. A number of routines to import the ANSYS model data and results were implemented in MATLAB.

The genetic algorithm is also implemented in MATLAB. All results presented in this paper are obtained using the Genetic Algorithm Optimization Toolbox - GAOT, developed by C.R Houck, J.A. Joines and M.G. Kay of North Carolina State University. This toolbox is free software which is available on the internet, see `http://www.ie.ncsu.edu/gaot`.

Test case

Setup. The setup used for the test case consists of a clamped rectangular plate with one surface bonded piezoelectric patch (see Fig. 2). The plate has dimensions $490 \times 245 \times 1.2$ mm^3. The disturbance input is a point force in the transverse direction applied at $(x, y) = (70, 154)$ mm. The control system consists of one actuator, the piezoelectric patch, one sensor, and the control algorithm described earlier. Three error criteria or sensor types are investigated: (1) radiated sound power $\bar{W}$, (2) structural normal displacement u_s, and, (3) acoustic nearfield pressure p_s. Obviously the first criterion is not very realistic, but it gives the best control performance, and is therefore used for comparison with the more realistic sensors. The control effort penalty β (see Eqs. (20, 21)) is zero for all three cases. Note that for all criteria the fitness function is the radiated sound power integrated over frequency (see Eq. (22)).

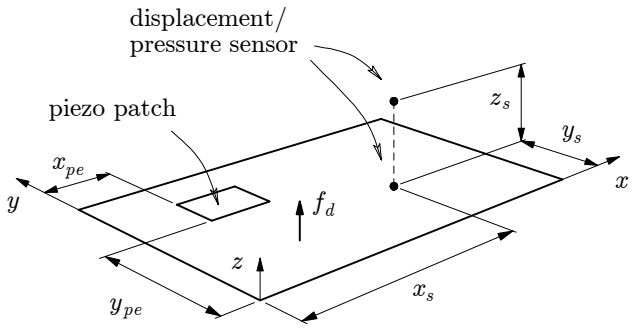

Figure 2: Clamped rectangular plate with one piezoelectric patch.

The number of design variables depends on the error criterion which is applied. For criterion (1), the actuator location, defined by x_{pe} and y_{pe}, is optimized. In case of the other criteria also the optimal sensor location is determined, i.e. (x_s, y_s) for criterion (2), and (x_s, y_s, z_s) for criterion (3). Note that in case of error criterion (3) the pressure is calculated with Eq. (15). The frequency range for optimization includes the first three structural mode shapes, and is given by $[\omega_0, \omega_1] = [70, 270]$ Hz. A number of 75 steps is used to evaluate the fitness function. The reduced structural and acoustical models are constructed with 12 structural modes and 10 radiation modes respectively.

Alternative placement method. The results which follow from genetic optimization will be compared with results obtained with an alternative method for actuator and sensor placement. This method uses the structural mode shapes of the plate without piezoelectric patch in the selection criterion. It it computationally much more efficient than genetic optimization, and is thus much more attractive for engineering application.

Analytical models of plates with surface bonded piezoelectric patch actuators (e.g. Dimitriadis et al [16]) show that the curvature of the plate is proportional to the strain induced by the patch. This means that a mode is best excited by a patch when it is placed at a location

corresponding with maximum curvature. The optimum is here defined as the location for which the function

$$\gamma(x,y) = \prod_{i=1}^{n_m} \frac{\hat{\kappa}_{x,i} + \hat{\kappa}_{y,i}}{\max(\hat{\kappa}_{x,i} + \hat{\kappa}_{y,i})}\,, \tag{27}$$

is maximal, where $\hat{\kappa}_{x,i}$ and $\hat{\kappa}_{x,i}$ are the curvature of mode i in x- and y-direction respectively. In the same way a criterion is defined to determine the displacement sensor location:

$$\beta(x,y) = \prod_{i=1}^{n_m} \frac{\hat{u}_i}{\max(\hat{u}_i)}\,. \tag{28}$$

The optimal locations have been obtained from plots of functions $\gamma(x,y)$ and $\beta(x,y)$ when using the analytical mode shapes of a clamped plate [17]. When three modes are included, i.e. $n_m = 3$, the optimal patch location is $(x_{pe}, y_{pe}) = (0.108, 0.108)$, and the optimal displacement sensor location is $(x_s, y_s) = (0.129, 0.123)$. Since Eqs. (27) and (28) only refer to the structural behaviour of the plate, no optimal microphone location can be determined with these criteria. The microphone is placed at the same location as the displacement sensor with an offset in z-direction of 100 mm.

Results

All results presented in this section have been obtained with a population of 25, and 50 generations. The number of crossover and mutation opertations per generation were 3 and 4 respectively. For each criterion three optimization runs were performed, the most optimal solutions are summarized in Tab. 1. The table gives besides the optimal locations also the corresponding fitness function value F_{Ga}, and the fitness function value F_{Alt} when the alternative placement method is applied. The differences between the results obtained with each optimization run are small for the actuator location (< 7 mm), but deviations up to 60 mm were found for the sensor location.

Error criterion	x_{pe}	y_{pe}	x_s	y_s	z_s	F_{Ga}	F_{Alt}
Sound power $\bar{W}$	0.0807	0.105	–	–	–	$8.72 \cdot 10^{-5}$	$7.63 \cdot 10^{-4}$
Displacement u_s	0.0801	0.101	0.228	0.112	–	$2.34 \cdot 10^{-4}$	$6.57 \cdot 10^{-1}$
Pressure p_s	0.0846	0.107	0.401	0.249	0.255	$8.90 \cdot 10^{-5}$	$1.91 \cdot 10^{-3}$

Table 1: *Optimization results.*

The passive response and active responses of the radiated sound power are compared in Fig. 3 for each error criterion. Two active response curves are shown in each figure, i.e. one corresponding with the actuator and sensor location which follow from the alternative placement method, and one corresponding with a control setup found with the genetic optimization strategy (see Tab. 1). Note that the fitness function value is equal to the area under these frequency response functions. The figure clearly shows that the control setup following from the genetic optimization strategy gives a larger reduction in radiated sound power than the setup found with the alternative placement method. This is especially the case for the displacement error criterion, see Fig 3(b). For this criterion the results corresponding with the alternative method

show a shift of the resonance frequencies. This behaviour, which is clarified in references [18, 19], and is related to the fact that a control system with one actuator and sensor is able to reduce the error signal to zero at each frequency. The control input must be very large at these resonance frequencies, and a non-zero control effort penalty will significantly change the behaviour. The vibration shape at such a resonance frequency corresponds with the mode shape found if the transverse displacement at the sensor location is suppressed. Shifting of resonance frequencies is also possible if the error sensor is a microphone, but this was not observed for the sensor locations here.

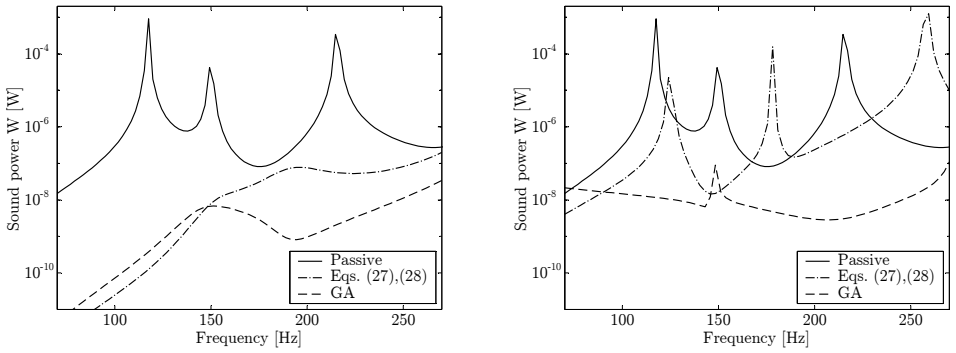

(a) Error criterion: $\bar{W}$

(b) Error criterion: u_s

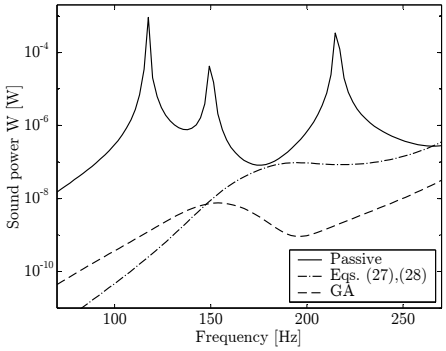

(c) Error criterion: p_s

Figure 3: *Comparison of optimal configurations for different error criteria: (a) radiated sound power $\bar{W}$, (b) out-of-plane displacement u_s, and, (c) near-field acoustic pressure p_s.*

Figure 4 compares the performance of the error criteria with corresponding optimal location of actuator and sensor. A remarkable aspect is that in the low frequency region the control system with one microphone gives a reduction in radiated power which is nearly equal to a controller which uses the sound power as error criterion. Outside of the optimization frequency range the control performance is not significant. Even an increase of radiated sound power can be observed for the displacement and pressure error criteria.

Conclusion

An optimization strategy for actuator and sensor placement in ASAC was presented. The strategy uses a dynamical model consisting of a structural dynamics model, sound radiation model and controller model. The FEM method is used to model the structural dynamics including

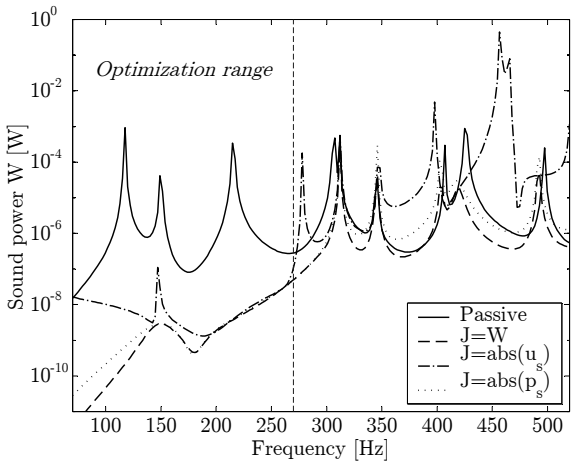

Figure 4: *Comparison of radiated sound power reduction for different error criteria.*

piezoelectric actuators (or sensors) and a reduction technique is applied to obtain fast simulation models. These features make the method more suitable for optimization of structures more complex than flat plates. The strategy uses a genetic algorithm to find optimal actuator and sensor locations, here with respect to minimum radiated sound power over a broad-band frequency range.

The optimization strategy was applied to a test case consisting of a clamped rectangular plate and control system with one piezoelectric patch actuator and one sensor. The actuator and sensor location were optimized and the results compared with an alternative method using only structural mode shapes. The optimization strategy clearly showed a larger reduction in radiated sound power. Future work focuses on experimental validation of the results found with the numerical study and extension to control systems with several actuators and sensors.

References

[1] C.R. Fuller. Active control of sound transmission/radiation from an elastic plate by vibration inputs: I. Analysis. *Journal of Sound and Vibration*, 136(1):1–15, 1990.

[2] R.L. Clark and C.R. Fuller. Optimal placement of piezoelectric actuators and polyvinylidene fluoride error sensors in active structural acoustic control approaches. *Journal of the Acoustical Society of America*, 92(3):1521–1533, 1992.

[3] B.-T. Wang, R.A. Burdisso, and C.R. Fuller. Optimal placement of piezoelectric actuators for active structural acoustic control. *Journal of Intelligent Material Systems and Structures*, 5(1):67–77, 1994.

[4] J. Kim, V.V. Varadan, and V.K. Varadan. Finite element-optimization methods for the active control of radiated sound from a plate structure. *Smart Materials and Structures*, 4(4):318–326, 1995.

[5] V.V. Varadan, J. Kim, and V.K. Varadan. Optimal placement of piezoelectric actuators for active noise control. *AIAA Journal*, 35(3):526–533, 1997.

[6] P. De Fonseca, P. Sas, and H. Van Brussel. A comparative study of methods for optimising sensor and actuator locations in active control applications. *Journal of Sound and Vibration*, 221(4):651–679, 1999.

[7] M.H.H. Oude Nijhuis and A. de Boer. Finite element models applied in active structural acoustic control. In *Proceedings of SPIE's 9th annual international symposium on Smart Structures and Materials*, San Diego, USA, 2002. To be published.

[8] A. Preumont. *Vibration control of Active Structures*. Kluwer Academic Publishers, 1999. ISBN 0-7923-4392-1.

[9] A.D. Pierce. *Acoustics, and Introduction to its Physical Principles and Applications*. Acoustical Society of America, 1994 edition edition, 1981.

[10] G.V. Borgiotti. The power radiated by a vibrating body in an acoustic fluid and its determination from boundary measurements. *Journal of the Acoustical Society of America*, 88(4):1884–1893, 1990.

[11] K.A. Cunefare and M.N. Currey. On the exterior acoustic radiation modes of structures. *Journal of the Acoustical Society of America*, 96(4):2302–2312, 1994.

[12] M.N. Currey and K.A. Cunefare. The radiation modes of baffled finite plates. *Journal of the Acoustical Society of America*, 98(3):1570–1580, 1995.

[13] P.A. Nelson and S.J. Elliott. *Active Control of Sound*. Academic Press, 1992. ISBN 0-12-515425-9.

[14] D.E. Goldberg. *Genetic Algorithms in Search, Optimization and Machine Learning*. Addison-Wesley, 1989. ISBN 0-201-15767-5.

[15] Z. Michalewicz. *Genetic Algortihms + Data Structures = Evolution Programs*. Springer-Verlag, 1994. ISBN 3-540-60676-9.

[16] E.K. Dimitriadis, C.R. Fuller, and C.A. Rogers. Piezoelectric actuators for distributed vibration excitation of thin plates. *Journal of Vibration and Acoustics*, 113(1):100–107, 1991.

[17] R.D. Blevins. *Formulas for Natural Frequency and Mode Shapes*. Robert E. Krieger Publishing, reprint edition edition, 1984. ISBN 0-89874-791-0.

[18] R.A. Burdisso and C.R. Fuller. Dynamic behavior of structural acoustic systems in feedforward control of sound radiation. *Journal of the Acoustical Society of America*, 92(1):277–286, 1992.

[19] R.A. Burdisso and C.R. Fuller. Theory of feedforward controlled system eigenproperties. *Journal of Sound and Vibration*, 153(?):437–451, 1992.